

Stacking Disorders in Mixed-Alkali Honeycomb Layered Oxide NaKNi₂TeO₆ and Feasibility for Mixed-Cation Transport

Titus Masese^{a,b}, Yoshinobu Miyazaki^c, Josef Rizell^{a,d}, Godwill Mbiti Kanyolo^e, Chih-Yao Chen^b, Kartik Sau^f, Tamio Ikeshoji^f, Zhen-Dong Huang^g, Kazuki Yoshii^a, Teruo Takahashi^c, Miyu Ito^c, Hiroshi Senoh^a, Kazuhiko Matsumoto^{b,h}, Rika Hagiwara^{b,h} & Tomohiro Saito^c

^a Research Institute of Electrochemical Energy, National Institute of Advanced Industrial Science and Technology (AIST), 1–8–31 Midorigaoka, Ikeda, Osaka 563–8577, JAPAN

Josef Rizell^{a,d}, Titus Masese^{a,b}, Kazuki Yoshii^b, Hiroshi Senoh^b

^b AIST-Kyoto University Chemical Energy Materials Open Innovation Laboratory (ChEM-OIL), Sakyo-ku, Kyoto 606–8501, JAPAN

Titus Masese^{b,d}, Chih-Yao Chen^d, Kazuhiko Matsumoto^{d,i}, Rika Hagiwara^{d,i}

^c Tsukuba Laboratory, Technical Solution Headquarters, Sumika Chemical Analysis Service (SCAS), Ltd., Tsukuba, Ibaraki 300–3266, JAPAN

Yoshinobu Miyazaki^a, Teruo Takahashi^a, Miyu Ito^a, Tomohiro Saito^a

^d Department of Physics, Chalmers University of Technology, SE–412 96 Göteborg, SWEDEN.
Josef Rizell^{a,d}

^e Department of Engineering Science, The University of Electro–Communications, 1–5–1 Chofugaoka, Chofu, Tokyo 182–8585, JAPAN

Godwill Mbiti Kanyolo^e

^f Mathematics for Advanced Materials - Open Innovation Laboratory (MathAM-OIL), National Institute of Advanced Industrial Science and Technology (AIST), c/o Advanced Institute of Material Research (AIMR), Tohoku University, Sendai 980–8577, JAPAN

Kartik Sau^f, Tamio Ikeshoji^f

^g Key Laboratory for Organic Electronics and Information Displays and Institute of Advanced Materials (IAM), Nanjing University of Posts and Telecommunications (NUPT), Nanjing, 210023, CHINA

Zhen-Dong Huang^g

^h Graduate School of Energy Science, Kyoto University, Sakyo-ku, Kyoto 606–8501, JAPAN
Kazuhiko Matsumoto^{b,h}, Rika Hagiwara^{b,h}

*Correspondence should be addressed to: Titus Masese (Lead contact)

E-mail address: titus.masese@aist.go.jp

Phone: +81–72–751–9224; Fax: +81–72–751–9609

Abstract

In this study, we demonstrate the feasibility of using a combination of alkali atoms (Na and K) to develop a robust mixed-alkali honeycomb layered oxide $\text{NaKNi}_2\text{TeO}_6$. Through a series of atomic-resolution transmission electron microscopy in multiple zone axes, we reveal for the first time the local atomic structural disorders characterised by aperiodic stackings and incoherency in the alternating arrangement of Na and K atoms. Our findings indicate great structural versatility that renders $\text{NaKNi}_2\text{TeO}_6$ an ideal platform for investigating other fascinating properties such as mixed ionic transport and intriguing electromagnetic and quantum phenomena amongst honeycomb layered oxides. Finally, we unveil the possibility of inducing mixed Na- and K-ion transport electrochemistry of $\text{NaKNi}_2\text{TeO}_6$ at high voltages ($\sim 4\text{V}$), thus epitomising it as a competent cathode candidate for the emerging dendrite-free batteries based on NaK liquid metal alloy as anodes. The results not only betoken a new avenue for developing functional materials with fascinating crystal versatility, but also prefigure a new age of ‘dendrite-free’ energy storage system designs that rely on mixed-cation electrochemistry.

INTRODUCTION

Honeycomb layered oxides are a family of lamellar-structured nanomaterials characterised by alkali or coinage metal atoms interleaved between sheets of transition metal atoms aligned in a honeycomb formation. This emerging class has been gaining momentous interest as a result of a smörgåsbord of appealing properties innate to their structural framework.^{1–10} The alkali- or coinage-metal atoms manifest weak interlayer bonds that engender an abundance of unoccupied sites that induce excellent ionic conductivities. This allows for facile reinsertion and extraction of alkali ions between the transition metal sheets, thus earmarking these materials as pedagogical exemplars of high-voltage cathodes for a novel class of rechargeable batteries.^{1,2,11–17} Furthermore, the sandwiching of non-magnetic atoms between a hexagonal sublattice comprising magnetic atoms results in pseudo-two-dimensional magnetic structures that have the potential to achieve exotic magnetic states with varied applications in fields such as quantum computing and solid-state physics.^{1,10}

Most honeycomb layered oxides encompass compositions; $A_2M_2DO_6$, $A_3M_2DO_6$ or A_4MDO_6 where A is an alkali- or coinage metal atom ($A = \text{Li, Na, K, Cu, Ag, ...}$), M is a transition metal atom ($M = \text{Ni, Co, Mg, Zn, Mn, Fe, Cr, ...}$) and D is a highly-valent ion like Te, Sb, Bi or W.¹¹ In these compositions, A atoms are sandwiched between slabs comprising M atoms surrounded by D atoms in a hexagonal formation. Depending on the atomic size of the A atom, the resulting lamellar structures manifest different sequential arrangements (hereupon referred to as stacking orders). Until now, only a handful of honeycomb layered oxides adopting T2-, O1-, O3- and P2-type (Hagenmuller-Delmas' notation) stacking orders have been identified, whereby 'T', 'O' and 'P' denote the tetrahedral, octahedral or prismatic coordination of oxygen with the A atoms, whilst the ensuing digit corresponds to the number of repeating transition metal layers in the unit cell.¹⁸ In order to further expand the scope of known honeycomb layered oxides and capitalise on their full potential, it is imperative to not only explore hitherto uncharted territories of their compositional space but also scrutinise their emergent stacking orders.

Amongst other classes of layered transition metal oxides, fascinating structures have been developed through the mixing of two different alkali species to formulate $A_xA'_yMO_2$ compositions. For instance, in the commonly studied $\text{Li}_x\text{Na}_y\text{CoO}_2$ layered cobaltate, the intermixing of similar amounts of Na and Li results in unique configurations of Na and Li within the different layers giving rise to versatile stacking structures ranging from OP4 to OPP9 stacking sequences.^{19,20} This structural versatility facilitates the development of

manifold crystal structures with myriad potential to host exquisite functionalities. Materials such as $\text{Li}_{0.48}\text{Na}_{0.35}\text{CoO}_2$ have been found to exhibit a large thermoelectric power (thermopower) at room temperature, surpassing that of either of its parent materials, Na_yCoO_2 and Li_xCoO_2 .²¹ Furthermore, the unique OP4 stacking sequence has found great utility in battery application as it allows $\text{Li}_x\text{Na}_y\text{CoO}_2$ to be utilised as a precursor in ion-exchange synthesis to create a new polymorph electrode material LiCoO_2 with O4-stacking.^{22,23}

Although the intermixing of alkali ions appears to be a judicious approach to the next level development of honeycomb layered oxides, as far as we can tell, only one report on a set of metastable antimonates $\text{Li}_{3-x}\text{Na}_x\text{Ni}_2\text{SbO}_6$ has been published on the topic.²⁴ Thus, in an attempt to gain deeper insights, herein we investigate a novel composition of $\text{Na}_{2-x}\text{K}_x\text{Ni}_2\text{TeO}_6$ honeycomb layered oxides. In this study, we utilise $\text{Na}_2\text{Ni}_2\text{TeO}_6$ and $\text{K}_2\text{Ni}_2\text{TeO}_6$ as the parent materials for the creation of a novel stable mixed alkali ion phase. The P2-type stacking (crystallising in the centrosymmetric $P6_3/mcm$ hexagonal space group) exhibited by both parent materials ($\text{Na}_2\text{Ni}_2\text{TeO}_6$ and $\text{K}_2\text{Ni}_2\text{TeO}_6$) is explicitly illustrated in **Figure 1a**, together with possible structural models for the resulting mixed compounds.

Furthermore, we unravel the structure of the new mixed alkali ion layered oxide $\text{NaKNi}_2\text{TeO}_6$ using atomic-resolution scanning transmission electron microscopy (STEM). Visualised for the *first time*, the local atomic structure reveals a unique and aperiodic stacking sequence in the layered mixed alkali ion compound. Moreover, we illustrate the potential of complex structures with intermixed alkali ions through electrochemistry and the conceptual demonstration of a dual cation battery using $\text{NaKNi}_2\text{TeO}_6$ as the cathode material that ideally matches both Na and K as the anode.

RESULTS

Mixed-alkali ion honeycomb layered oxides adopting the composition of $\text{Na}_{2-x}\text{K}_x\text{Ni}_2\text{TeO}_6$ ($0 \leq x \leq 2$) were synthesised via a high-temperature solid-state synthesis route described in the **METHODS** section. A preliminary characterisation of the average crystal structures of the as-synthesised (pristine) materials was carried out using powder X-ray diffraction (XRD) (as shown in **Figure 1b**). When the smaller Na atoms were replaced with larger K atoms (*viz.*, increasing x from 0 to 2), a stepwise shift comprised of several diffraction peaks was observed. Particularly, three discrete shifts are seen 00/ peaks of the $\text{Na}_{2-x}\text{K}_x\text{Ni}_2\text{TeO}_6$ as shown in **Figure 1c**. Since the diffraction angles of the 00/ peaks are inversely proportional to the distance between adjacent transition metal slabs (hereafter referred to as the interlayer distance), each position corresponds to a phase with a different interlayer distance. Two of the phases have interlayer distances closely resembling the parent materials $\text{Na}_2\text{Ni}_2\text{TeO}_6$ and $\text{K}_2\text{Ni}_2\text{TeO}_6$, whilst the last phase has an intermediate interlayer distance, indicating the existence of both Na and K atoms in this phase.

It should also be noted that, amongst the $\text{Na}_{2-x}\text{K}_x\text{Ni}_2\text{TeO}_6$ diffraction patterns, peaks previously not found in the parent materials were observed in the mixed alkali compound. As illustrated by **Figure 1d**, a peak located at lower diffraction angles emerges in the intermediate compositions despite being forbidden in the $P6_3/mcm$ hexagonal space group used to index both $\text{Na}_2\text{Ni}_2\text{TeO}_6$ and $\text{K}_2\text{Ni}_2\text{TeO}_6$. Similar observations have been noted on a previous report on $\text{Li}_{3-x}\text{Na}_x\text{Ni}_2\text{SbO}_6$ whereby disparate peaks emerged when Li and Na atoms were separated in different layers,²⁴ suggesting new cationic ordering in these new materials. As such, the disappearance of the 102 Bragg peak and the emergence of a new set of peaks in close proximity underline the structural changes occurring in this intermediate phase.

In order to quantify and better illustrate how the lattice parameters of the phases present in $\text{Na}_{2-x}\text{K}_x\text{Ni}_2\text{TeO}_6$ change with varying amounts of Na and K, profile fitting (Le Bail fit) of the XRD patterns was subsequently carried out. The average lattice parameters as deduced from the fit, are provided in the Supplementary Information (**Figure S1**). $\text{Na}_{2-x}\text{K}_x\text{Ni}_2\text{TeO}_6$ compositions where $0.2 \leq x \leq 1.8$ are treated as two-phase mixtures, since the 00/ Bragg peaks split into two separate peaks in these samples (as shown in **Figure 1c**). When K content (x , in $\text{Na}_{2-x}\text{K}_x\text{Ni}_2\text{TeO}_6$) is increased with $\text{Na}_2\text{Ni}_2\text{TeO}_6$ as the starting material, the relative intensity of the peaks corresponding to the $\text{Na}_2\text{Ni}_2\text{TeO}_6$ phase decrease in favour of the new intermediate phase. When an equimolar ratio of Na and K

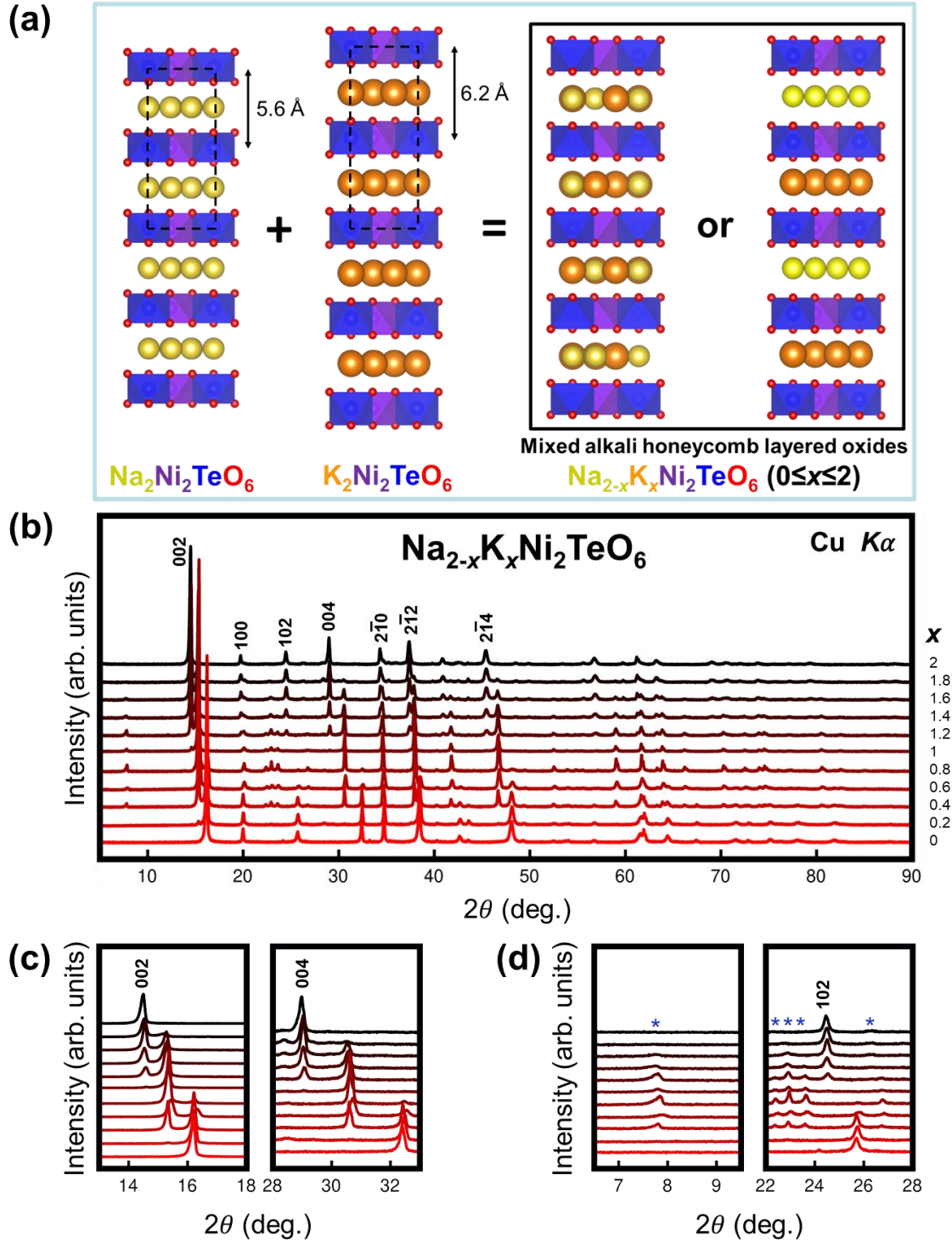


Figure 1. X-ray diffraction (XRD) analyses of $\text{Na}_{2-x}\text{K}_x\text{Ni}_2\text{TeO}_6$ ($0 \leq x \leq 2$). (a) Schematic illustration of possible structural models in mixed alkali atom honeycomb layered oxides adopting the composition $\text{Na}_{2-x}\text{K}_x\text{Ni}_2\text{TeO}_6$ ($0 \leq x \leq 2$). In the isostructural $\text{A}_2\text{Ni}_2\text{TeO}_6$ ($\text{A} = \text{Na}, \text{K}$) compounds, Na atoms (in yellow) or K atoms (in orange) are

sandwiched between layers or slabs consisting exclusively of TeO_6 (blue) and NiO_6 (purple) octahedra. Black dashed lines denote the unit cell. Owing to the larger Shannon-Prewitt ionic radius of K^+ (1.38 Å) compared to Na^+ (1.02 Å), the interlayer distance of $\text{K}_2\text{Ni}_2\text{TeO}_6$ is significantly larger than that of $\text{Na}_2\text{Ni}_2\text{TeO}_6$. Various reasonable structural models can be hypothesised for the new series of compounds adopting the composition $\text{Na}_{2-x}\text{K}_x\text{Ni}_2\text{TeO}_6$ ($0 \leq x \leq 2$). Here, models where Na and K atoms are either mixed within the same layers or separated into different layers are shown. **(b)** XRD patterns of as-synthesised $\text{Na}_{2-x}\text{K}_x\text{Ni}_2\text{TeO}_6$ ($0 \leq x \leq 2$), showing a stepwise shift of Bragg peaks towards lower diffraction angles with the substitution of Na with K. Bragg peaks for $\text{K}_2\text{Ni}_2\text{TeO}_6$ that are indexed in the hexagonal $P6_3/mcm$ space group are shown in black. **(c)** A stepwise shift of the 002 and 004 Bragg peaks that clearly hallmark the increase in the interlayer distance with K atom substitution. The three distinct peak positions correspond to three phases with different interlayer distances (along the c -axis), with the intermediate peak position signifying the formation of a new phase that is different from the end members $\text{Na}_2\text{Ni}_2\text{TeO}_6$ and $\text{K}_2\text{Ni}_2\text{TeO}_6$. **(d)** Emergence of new Bragg peaks in the intermediate compositions ($0 \leq x \leq 2$), which are not allowed in the $P6_3/mcm$ hexagonal space group. These new peaks are marked by asterisks and are indicative of a symmetry change that may entail the formation of superstructures.

is reached (*i.e.*, $\text{NaKNi}_2\text{TeO}_6$), the $\text{Na}_2\text{Ni}_2\text{TeO}_6$ peaks disappear and a weak $\text{K}_2\text{Ni}_2\text{TeO}_6$ peak emerges. With further increase in the K content, the relative intensities of the peak corresponding to the intermediate phase decreases accordingly until pure $\text{K}_2\text{Ni}_2\text{TeO}_6$ is attained.

The tendency of these mixed-alkali ion compositions to separate into two-phase mixtures can be rationalised by the large difference in the Shannon-Prewitt ionic radii of Na^+ and K^+ ,²⁵ that make it difficult to form a solid-solution compound from a mixture of $\text{Na}_2\text{Ni}_2\text{TeO}_6$ and $\text{K}_2\text{Ni}_2\text{TeO}_6$. Similar behaviour has also been observed amongst the layered nickelates $\text{Na}_x\text{Li}_{1-x}\text{NiO}_2$, where three different polymorphs with intermediate two-phase regions form depending on the stoichiometric Li/Na ratio, presumably as a result of the large difference between the ionic radii of Li and Na.²⁶ To further elucidate the manner of alkali atom arrangement upon successful intermixing of Na and K and the corresponding structural changes previously indicated by the XRD patterns (**Figure 1d**), electron microscopy was employed on $\text{NaKNi}_2\text{TeO}_6$ whose composition is closest to a phase-pure sample

The atomic-resolution imaging was accomplished using an aberration-corrected scanning transmission electron microscopy (STEM). From the [001] zone axis, the characteristic honeycomb arrangement of transition metal atoms can be observed. **Figure 2a** shows a high-angle annular dark field (HAADF)-STEM image of the parent compound $\text{K}_2\text{Ni}_2\text{TeO}_6$. As the intensity is approximately proportional to the square of the atomic number (hereafter as Z),^{27–29} the honeycomb arrangement of heavier elements Te ($Z = 52$) and Ni ($Z = 28$) should be explicitly visualised through spots of varying intensities, as revealed for the analogous $\text{K}_2\text{Ni}_2\text{TeO}_6$ (see **Figure S2**), with red spots marking columns of Ni atoms whilst bright yellow spots correspond to Te atoms columns. As such, it should be possible to acquire an analogous image for $\text{NaKNi}_2\text{TeO}_6$, if the honeycomb slab structure of $\text{NaKNi}_2\text{TeO}_6$ is similar to that of $\text{K}_2\text{Ni}_2\text{TeO}_6$. However, **Figure 2a** shows that all atomic sites in the image share the same intensity due to overlapping Ni and Te atoms in adjacent layers. It was also elusive to discern lighter (lower atomic mass) elements such as K and Na, in the corresponding annular bright-field (ABF)-STEM images (shown in **Figure 2b**).

To ascertain the structural changes responsible for the overlapping Ni and Te atoms observed in $\text{NaKNi}_2\text{TeO}_6$, the crystallites were examined from different directions (zone axes). A view from the [100] direction reveals the lamellar nature of the structure. In the HAADF-STEM image (**Figure 2c**), the Te and Ni atoms correspond to a set of bright planes. This assignment was further confirmed by augmenting the STEM images with energy dispersive X-ray diffraction (EDX), as shown in **Figure S3**. Elemental mapping using EDX also reveals that Na and K atoms are sandwiched between these Ni/Te-slabs. The images further reveal that Na and K are separated into different layers, rather than randomly mixed within the same layers (**Figures 2d-f**).

Further analyses from the [100] direction using atomic-resolution STEM images allow the stacking order in $\text{NaKNi}_2\text{TeO}_6$ to be characterised. Notably, the shifts between adjacent Ni/Te slabs are contingent on whether the interlayer spaces are occupied by Na or K atoms (**Figure 2g**). No shifts are observed when Ni/Te slabs are separated by a K layer. The same alternating arrangement of Na and K atom layers was observed also when viewed along the [1-10] zone axis, as shown in **Figure S4**. However, the transition metal slabs between which Na atoms reside, the metal slabs shift by 1/3 period along or parallel the slabs. This stacking shift explains the overlapping Ni and Te atoms observed from the [001] direction (**Figures 2a and 2b**). There seems to be no periodicity in the direction of

the slab shifts, and it seems to be almost random.

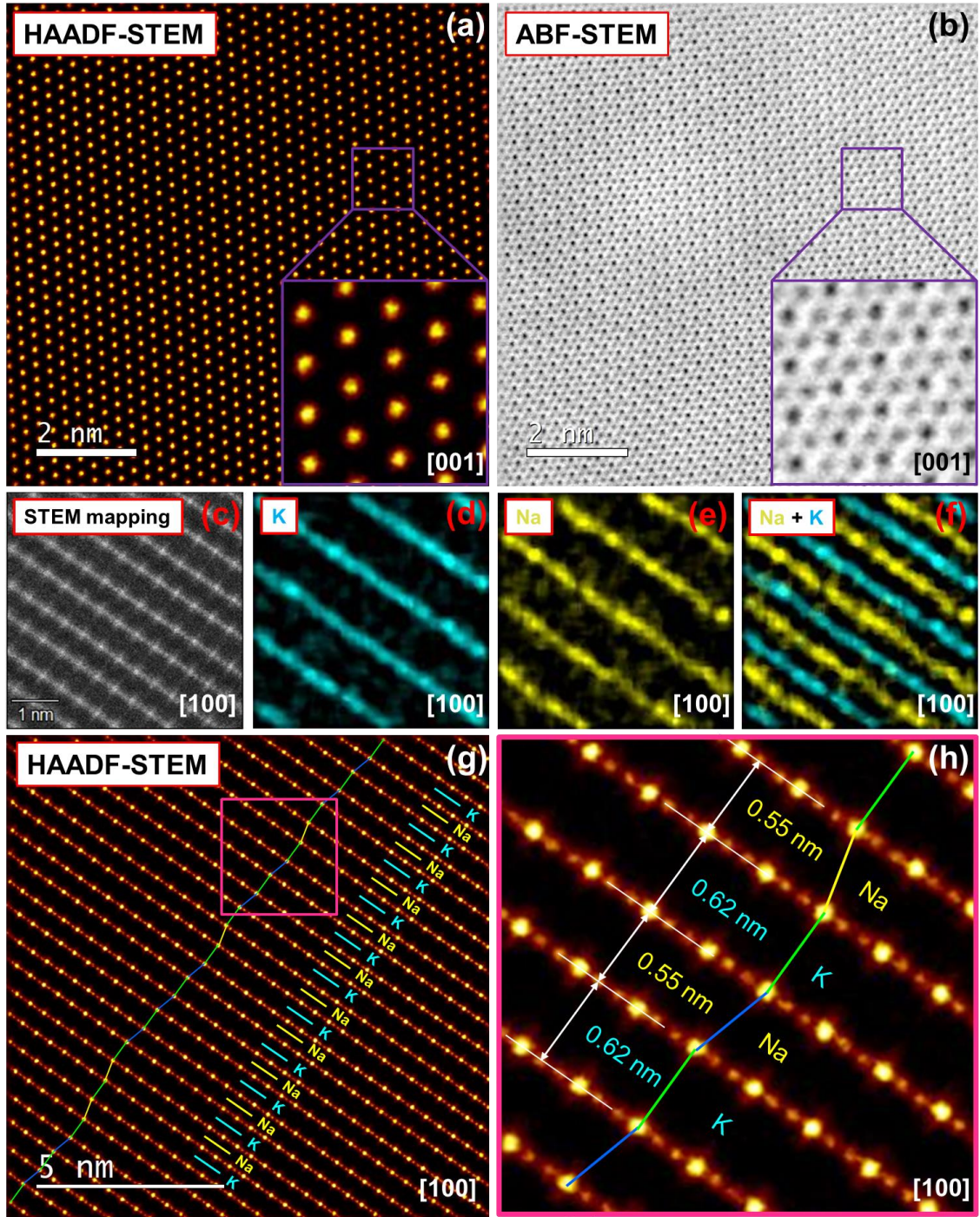


Figure 2. Arrangement of atoms in NaKNi₂TeO₆, viewed along the [001] and [100] directions. (a) High-angle annular dark-field (HAADF) scanning transmission electron microscopy (STEM) images taken along the [001] zone axis. Overlap of Te and Ni atom positions in the adjacent layers along the *c*-axis result in spots with uniform intensity (when viewed in the [001] zone axis). (b) Corresponding annular bright-field (ABF)-

STEM image, where also lighter elements (Na, K and O) can be visualised. **(c)** HAADF-STEM image of $\text{NaKNi}_2\text{TeO}_6$ taken along the $[100]$ zone axis, revealing bright planes corresponding to the layers comprising Te and Ni, as further explicated in the corresponding energy dispersive X-ray (EDX) imaging (see **Supplementary Information (Figure S3)** section). **(d, e and f)** STEM-EDX mapping of the area shown in **(a)**, where the colours explicitly visualise the distribution of Na and K atoms. The EDX maps show that the layers occupied by Na alternate with those of K. **(g)** HAADF-STEM image illustrating the unique stacking sequence in $\text{NaKNi}_2\text{TeO}_6$. In the layers where K atoms occupy the interlayer space, Te / Ni slabs are not shifted with respect to each other (marked by a green line). However, for layers where Na atoms reside, $\pm 1/3$ shifts of the Te / Ni slabs are observed. The yellow and blue lines show shifts in different directions. Note the aperiodicity in the stacking sequence. **(h)** Enlarged view of the domain highlighted in **(e)**, showing that the interlayer distance is contingent upon the alkali atom species (Na or K) sandwiched between the Te / Ni layers.

Attempts to ascertain whether it is a truly random structure or an aperiodic but ordered structure at some degree, proved elusive. From an enlarged view of the atomic-scale HAADF-STEM mapping (**Figure 2h**), it is also evident that the interlayer distance depends on the alkali atom species sandwiched between adjacent Ni/Te layers. The Ni/Te layers with Na atoms are separated by 0.55 nm (5.5 Å) whilst the interlayer distance for the layers with K is 0.62 nm (6.2 Å). It is worth highlighting that these interlayer distances attained closely resemble those of the parent compounds $\text{Na}_2\text{Ni}_2\text{TeO}_6$ and $\text{K}_2\text{Ni}_2\text{TeO}_6$ (**Figure 1a**). Exclusively relying on the XRD patterns only yields the average of these interlayer spacings/distances (**Figure S1**), accentuating the benefit of using TEM to obtain important structural information.

Although the atomic structure of $\text{NaKNi}_2\text{TeO}_6$ exhibits significant aperiodicity, a partial structural model containing the slab shift can still be constructed based on the TEM analysis. The atomic coordinates of the model were also based on $\text{K}_2\text{Ni}_2\text{TeO}_6$ structure obtained from XRD analysis. **Figure 3a** illustrates an atomistic model viewed from the $[100]$ direction. The model can be superimposed on both HAADF-STEM and ABF-STEM images, to confirm the accuracy of the positions of both heavier and lighter elements (**Figures 3b-c**). A comparison between the average structure model and a

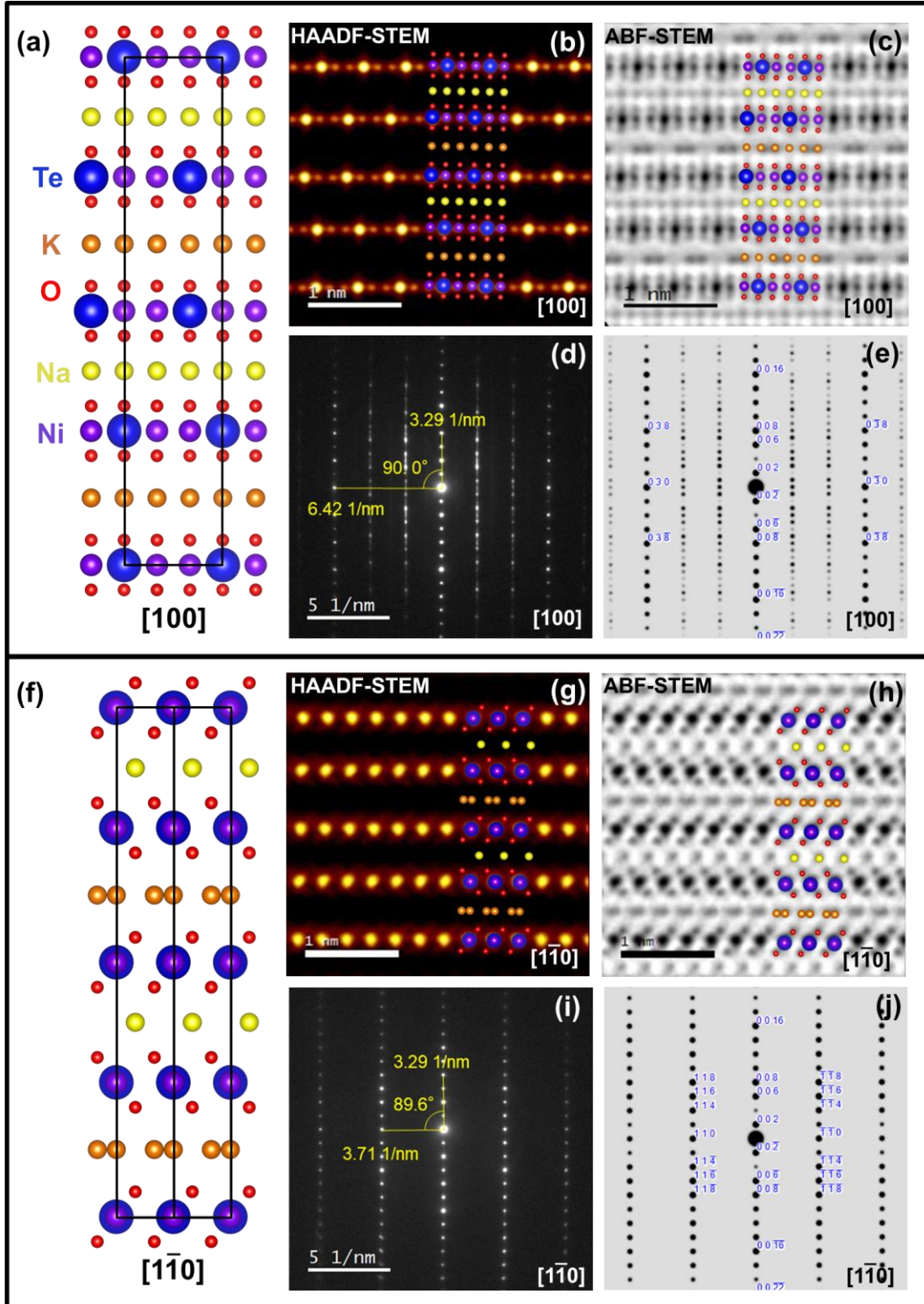


Figure 3. Aperiodic atomic structure of NaKNi₂TeO₆ along the [100] and the [1-10] zone axes. (a) Atomistic model of the average aperiodic structure of NaKNi₂TeO₆ acquired based on STEM analyses along the [100] zone axis. Black lines show the partial

unit cell. **(b)** Superimposition of the model on a HAADF-STEM image, showing an excellent overlap between the positions of the Ni and Te atoms in the model that is in accord with the intensity distribution of the atom spots observed in the image. **(c)** Superimposition of the model on an annular dark-field (ADF) image, affirming the atomic positions of Na, K and O. **(d)** Selected area electron diffraction (SAED) patterns taken along the [100] zone axis revealing spot shifts and streaks that are suggestive of the existence of aperiodicity. **(e)** Corresponding kinematic simulations based on the structural model shown in **(a)**, showing agreement with the experimental results in **(d)**. **(f)** Atomistic model of NaKNi₂TeO₆ acquired based on STEM analyses along the [1-10] zone axis. Black lines show the partial unit cell. Note the difference in the arrangement of atoms between Na (yellow) and K (orange) crystallographic sites. **(g)** Superimposition of the model on a HAADF-STEM image, affirming the atomic positions of Ni and Te. **(h)** Superimposition of the model on an ABF-STEM image, also showing an excellent overlap between the positions of the Na, K and O atoms in the model that is in accord with the intensity distribution of the atom spots observed in the image. **(i)** SAED patterns taken along the [1-10] zone axis and **(j)** the corresponding kinematic simulations, validating good agreement with the experimental results shown in **(d)**.

kinematically simulated selected area electron diffraction (SAED) pattern was drawn to provide further evidence on the validity of the obtained model (**Figures 3d-e**). The overall appearance of the simulation based on our model seems similar to the ones observed in the experiment, indicating that the partial model represents the average structure relatively well. However, deviation of the peaks from the periodic arrangement and the presence of streaks along the [001] direction in the experimental SAED patterns (**Figure 3d**), attest to the aperiodic stacking sequence previously described.

To fully capture the atomistic model of NaKNi₂TeO₆, analyses along the [1-10] zone axes are complementary, as shown in the partial structure model (**Figure 3f**). The model was superimposed on both ABF-STEM and HAADF-STEM images, yields excellent resemblance thus confirming the accuracy of the alkali atom sites in the model. The position of Ni and Te atoms are also clearly distinguished in the HAADF-STEM image (**Figure 3g**). It should be noted that the shift of the metal slabs that was observed for all Na layers in the [100], was not observed in the [1-10] direction. This reveals that the slab shift can be described as $[\pm 2/3 \ \pm 1/3 \ 0]$, that is, it corresponds to the swapping of Ni

and Te site, and explains the fact that Ni and Te were indistinguishable in the [001] observation. Correspondingly, in the ABF-STEM superimposition, the Na and K atoms are seen as bright grey spots between the darker Te/Ni-atom planes (**Figure 3h**). A clear difference between Na and K atom sites can be identified. The prismatic coordination of oxygen is clearly seen in the ABF-STEM images in both the Na and K layers. However, Na-atom sites are equidistantly spaced, whilst two adjacent K atom sites are grouped together.

SAED patterns in the [1-10] direction generated in a kinematic simulation based on the model agree well with the experimentally determined diffraction pattern (**Figures. 3i-j**). No streaks or peak deviations from periodic arrangement are observed in the diffraction pattern from the [1-10] zone axes (**Figure 3i**) as opposed to the [100] direction (**Figure 3d**). It validates that [1-10] projected structure is completely periodic since the shift of Ni/Te layers possessing the aperiodicity occurs along this direction.

DISCUSSION

A detailed characterisation of the crystal structure of a new mixed-alkali honeycomb layered oxide ($\text{NaKNi}_2\text{TeO}_6$) was achieved using aberration-corrected STEM. To our knowledge, previous reports on the local atomic structure of a mixed-alkali ion layered oxide with similar structure have not been previously reported, making information on this class of materials obscure and underutilised. In the course of this study, a prominent aspect that emerges is the difference between Na and K sites evident when $\text{NaKNi}_2\text{TeO}_6$ crystals are viewed along the [1-10] and [100] zone axes. We find that, Na atoms are distributed in sites that assume triangular patterns (**Figure 4a**) whilst the K atoms reside in sites arranged in honeycomb formations (**Figure 4b**). Although beyond the limits of present experiments, these atomic configurations and crystallographic occupations can be used to predict emergent properties of such materials as well as the electrodynamics of the alkali or coinage atoms within the realm of their electromagnetic behaviour, electrochemistry, quantum phenomena, *etc.*³⁰ For instance, the atomic arrangements of the atoms given in **Figure 4a** and **Figure 4b** are intricately linked to crystalline entropy considerations (see **Supplementary Note 1**). This, in turn, can be envisaged to impact the electrodynamics of alkali ions in the material.

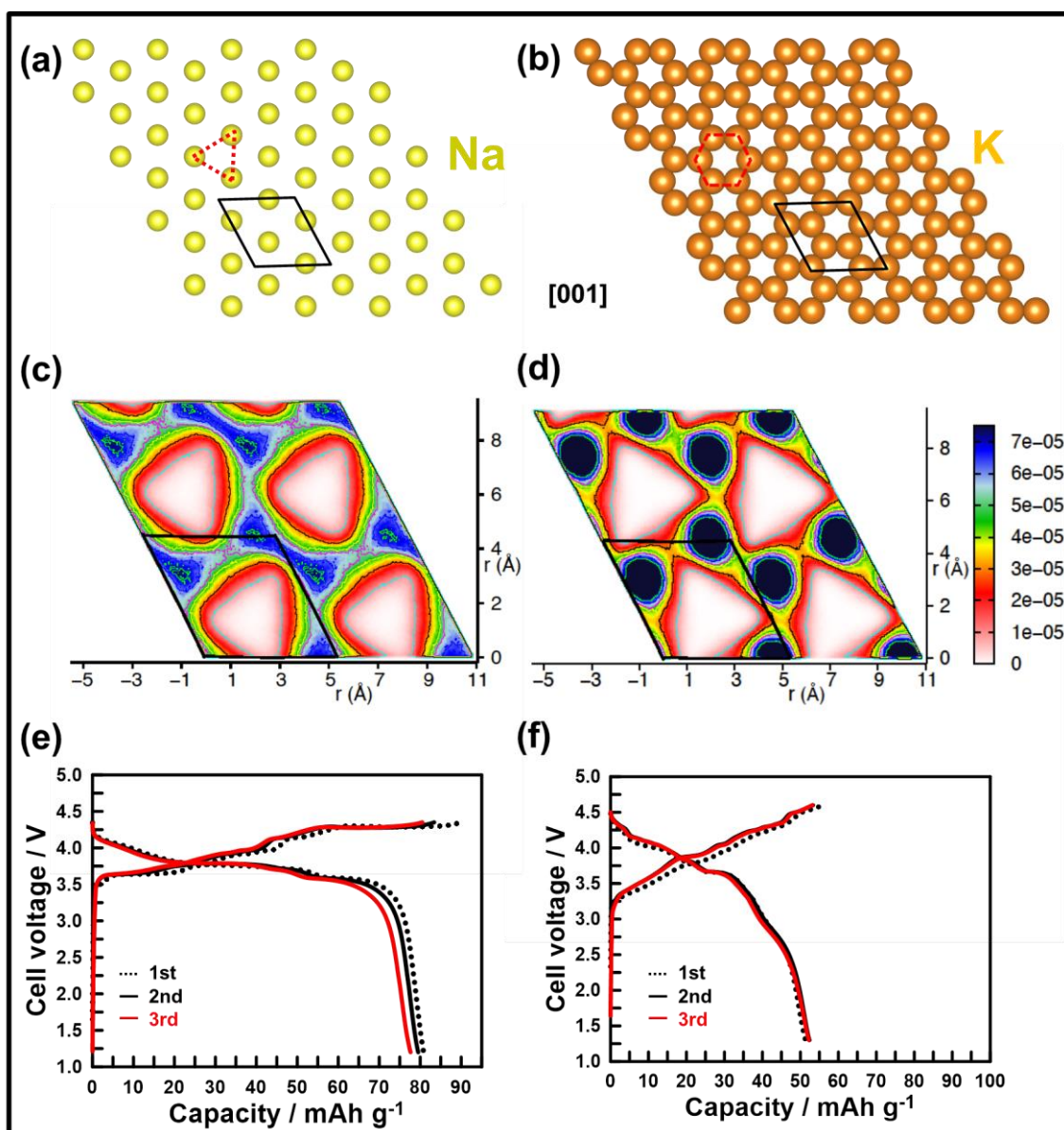


Figure 4. Mixed alkali ion transport in NaKNi₂TeO₆. (a) Arrangement of the Na atoms in triangular sites (as highlighted in red) as viewed along the [001] zone axis. The unit cell is highlighted in black lines. For the sake of clarity, the atoms denote the conformation of the sites and not the occupancy. (b) Honeycomb arrangement of K atoms in their respective sites as depicted along the [001] zone axis. (c) Molecular dynamics (MD) simulation showing the Na⁺ ion probability density profile in the Na-layer (mapped onto 2 × 2 unit cells) using common colour bars (shown on the right). The population contours reflect the preferred migration pathway amongst the interstitial cationic sites. (d) MD simulation for K⁺ ion probability density profile in the K-layer. (e) Voltage-capacity profiles of NaKNi₂TeO₆ in Na-half cells using 1 M NaFSI in *N*-methyl-*N*-propylpyrrolidinium-based (Pyrr₁₃FSI) ionic liquid and (f) K-half cells using 1 M KFSI

in Pyr₁₃FSI ionic liquid. A current density of 6.65 mA g⁻¹ commensurate to (dis)charging for 20 hours to a full theoretical two-electron capacity (*viz.* C/20 rate) was used.

Molecular dynamics (MD) simulations can avail insights into the microscopic alkali-ion transport of functional materials. This information is useful to gauge the feasibility of NaKNi₂TeO₆ as an energy storage material. MD simulations were performed based on the X-ray structure of NaKNi₂TeO₆, details of which are provided in the **METHODS** section. Computing the mean squared displacement at 600 K, we find that Na⁺ ion has a higher diffusion coefficient (D) than K⁺ ion based on the equation $\lim_{t \rightarrow \infty} \frac{1}{t} \langle [\Delta r(t)]^2 \rangle = 4Dt$, (where t is the time variable and $\Delta r(t)$ is the displacement of the cation) inside the conduction layer as is evident in **Supplementary Figure S5**. The Na⁺ and K⁺ ion population profile displayed in **Figures 4c** and **4d** also show the similar behavior within the structure of NaKNi₂TeO₆. A few high-density areas are identified in the population profile, indicating favourable sites of Na⁺ or K⁺ ions. Particularly, the high-density areas are well-connected for the Na-layer, whereas a modest connectivity amongst the high-density sites in K-layer is observed, resulting in higher diffusion of Na⁺ ion compared to K⁺ ion. It is worth to mention that this behaviour is different than the parent Na or K-systems *i.e.* A₂Ni₂TeO₆, where $A = \text{Na, K}$. This can be traced to the vastly different NiO₆ and TeO₆ octahedral stacking sequences from the parent Na or K-systems, which leads to a differing local environment.^{1,44} Recall, we observed in STEM (**Figure 2g**) that, the layers where K atoms occupy the interlayer space, Te / Ni slabs are not shifted with respect to each other whereas, for layers where Na atoms reside, shifts of the Te / Ni slabs are observed. This behaviour is maintained in the simulation results despite high temperatures where the alkali ions are dynamic (see **Supplementary Video 1**). Further investigation of the nature of Na and K ion transport and its mechanism is beyond the scope of this work.

Presumably, NaKNi₂TeO₆ like other honeycomb layered oxides, holds potential in many fields. Nonetheless, the primary focus of this study is to ascertain its feasibility as a rechargeable battery electrode material. Thus, alkali-ion electrochemical tests were conducted to verify its capability to facilitate mixed-alkali ion extraction and insertion. Subsequently, separate Na and K half-cells were assembled, as further explicated in the **METHODS** section. **Figure 4c** shows the voltage-capacity plots of NaKNi₂TeO₆ in Na half-cells. The theoretical capacity for a full Na⁺ extraction from NaKNi₂TeO₆ is

approximately 67 mAh g^{-1} . However, a reversible capacity of *ca.* 80 mAh g^{-1} was attained upon subsequent cycling, suggesting the occurrence of K^+ extraction. In the case of the K half-cells (**Figure 4d**), an initial capacity of 45 mAh g^{-1} was realised and maintained upon successive cycling. This capacity presumably arises from predominant K^+ extraction given that K metal was used. These electrochemical measurements indicate that $\text{NaKNi}_2\text{TeO}_6$ mixed-alkali honeycomb layered oxide is amenable to binary alkali-ion electrochemistry, pointing towards the possibility of developing a viable mixed Na- and K-ion electrochemical cell that relies on electrolytes and electrode materials that can accommodate both Na and K binary-cation transport.

Given that batteries utilising both cation and anion as charge carriers (dual-ion batteries (DIBs)) have already shown remarkable metrics in terms of energy density, power density and cycling life,^{42,46–48} the present battery chemistry exploiting binary alkali metal cations could be a promising successor to DIB technology. By exploiting the synergistic effect of Na- and K-ion electrochemistry, the battery confers the aforementioned metrics besides taking advantage of the abundance of Na and K resources. Moreover, it offers the possibility of utilising a NaK liquid metal alloy as anode material which is very effective in accommodating the cations, thwarting the formation of dendrites that have long plagued the direct utilisation of alkali metal anodes in secondary batteries (as succinctly demonstrated in **Figure S6**).

It is imperative to mention that although the concept of mixed-alkali battery materials is not unprecedented, it has been found to ameliorate some battery functionalities. For instance, the substitution of Li atoms in layered transition metal cathode oxides with miniscule amounts of Na, K, Rb or Cs is a well-investigated route to enhance their structural stability and increase Li-ion diffusion.^{31–39} However, the theoretical capacity of materials with similar amounts of different alkali metal atoms, such as $\text{NaKNi}_2\text{TeO}_6$, is drastically attenuated when large amounts of Na are replaced with K in a cathode for a Na-battery or *vice versa*. This is generally ascribed to the fact that the number of cations participating in extraction and reinsertion would be diminished. As a way to enhance performance, the utilisation of an alloy such as NaK in the case of $\text{NaKNi}_2\text{TeO}_6$ would facilitate the participation of both cation species thus yield a realistic theoretical capacity, as demonstrated in **Figure S6**. In addition, the liquid nature of NaK does not allow the formation of dendrite on the anode thus rendering the design ‘a dendrite-free’ metal anode battery. Therefore, this concept showcases the potential for $\text{NaKNi}_2\text{TeO}_6$ and related mixed-alkali layered oxide materials as functional materials.

Motivated by the projected functionalities of such materials, attempts were made to synthesise various compositions that form structures akin to those of NaKNi₂TeO₆. Partial substitution of Ni with Co, lead to the successful synthesis of mixed-alkali layered oxides adopting the compositions Na_{2-x}K_xNi_{2-y}Co_yTeO₆ ($y = 0.25, 0.5, 0.75, 0.1$) (as shown in **Figures S7-S9**). Material characterisation using XRD data confirm the formation of intermediate phases regardless of the extent of Co-doping, highlighting the possibility to create structures similar to that of NaKNi₂TeO₆ in other compositions.

In conclusion, the successful design of mixed-alkali honeycomb layered oxides, for instance NaKNi₂TeO₆, not only offers a conduit to engineering new functional materials but also promises to expand the compositional space of known honeycomb layered oxides. The results of this study suggest a correlation between the ionic radii of the alkali atoms and the interlayer distance, which can be exploited to configure the intricate interlayer structure of the mixed-alkali honeycomb layered oxides, by the same token as Ag/LiCoO₂.⁴⁰ Detailed local atomic information provided through a series of scanning transmission electron microscopy (STEM) reveal characteristics of an unique aperiodic stacking structure, suggesting structural versatility that could unlock the potential of this material for fascinating electromagnetic, quantum and electrochemical functionalities.^{1,30,41} Further, we expound on the feasibility of NaKNi₂TeO₆ for battery applications that utilise mixed cation transport. The mixed triangular and honeycomb atomics conformations may have profound impact on the electrodynamics of the alkali ions. An attempt to rationise this view has been made by theoretical computations. We hope that this work will serve as a cornerstone for further augmentation of mixed-alkali layered oxides in various realms of science and technology.

References

1. Kanyolo, G. M. *et al.* Honeycomb Layered Oxides: Structure, Energy Storage, Transport, Topology and Relevant Insights. arXiv. arXiv:2003.03555 (2020).
2. Masese, T. *et al.* Rechargeable potassium-ion batteries with honeycomb-layered tellurates as high voltage cathodes and fast potassium-ion conductors. *Nat. Commun.* **9**, 3823 (2018).
3. Masese, T. *et al.* A high voltage honeycomb layered cathode framework for rechargeable potassium-ion battery: P2-type K_{2/3}Ni_{1/3}Co_{1/3}Te_{1/3}O₂. *Chem. Commun.* **55**, 985–988 (2019).

4. Yang, Z. *et al.* A high-voltage honeycomb-layered $\text{Na}_4\text{NiTeO}_6$ as cathode material for Na-ion batteries. *J. Power Sources* **360**, 319–323 (2017).
5. Yuan, D. *et al.* A Honeycomb-Layered $\text{Na}_3\text{Ni}_2\text{SbO}_6$: A High-Rate and Cycle-Stable Cathode for Sodium-Ion Batteries. *Adv. Mater.* **26**, 6301–6306 (2014).
6. Sathiya, M. *et al.* $\text{Li}_4\text{NiTeO}_6$ as a positive electrode for Li-ion batteries. *Chem. Commun.* **49**, 11376–11378 (2013).
7. Bhange, D. S. *et al.* Honeycomb-layer structured $\text{Na}_3\text{Ni}_2\text{BiO}_6$ as a high voltage and long life cathode material for sodium-ion batteries. *J. Mater. Chem. A* **5**, 1300–1310 (2017).
8. Yoshii, K. *et al.* Sulfonamide-Based Ionic Liquids for High-Voltage Potassium-Ion Batteries with Honeycomb Layered Cathode Oxides. *ChemElectroChem* **6**, 3901–3910 (2019).
9. Wang, P.-F. *et al.* An Ordered Ni_6 -Ring Superstructure Enables a Highly Stable Sodium Oxide Cathode. *Adv. Mater.* **31**, 1903483 (2019).
10. Kitaev, A. Anyons in an exactly solved model and beyond. *Ann. Phys. (N. Y.)* **321**, 2–111 (2006).
11. Evstigneeva, M. A., Nalbandyan, V. B., Petrenko, A. A., Medvedev, B. S. & Kataev, A. A. A new family of fast sodium ion conductors: $\text{Na}_2\text{M}_2\text{TeO}_6$ ($M = \text{Ni}, \text{Co}, \text{Zn}, \text{Mg}$). *Chem. Mater.* **23**, 1174–1181 (2011).
12. Nalbandyan, V. B., Petrenko, A. A. & Evstigneeva, M. A. Heterovalent substitutions in $\text{Na}_2\text{M}_2\text{TeO}_6$ family: Crystal structure, fast sodium ion conduction and phase transition of $\text{Na}_2\text{LiFeTeO}_6$. *Solid State Ionics* **233**, 7–11 (2013).
13. Kumar, V., Bhardwaj, N., Tomar, N., Thakral, V. & Uma, S. Novel Lithium-Containing Honeycomb Structures. *Inorg. Chem.* **51**, 10471–10473 (2012).
14. Li, Y. *et al.* New P2-Type Honeycomb-Layered Sodium-Ion Conductor: $\text{Na}_2\text{Mg}_2\text{TeO}_6$. *ACS Appl. Mater. Interfaces* **10**, 15760–15766 (2018).
15. Wu, J.-F., Wang, Q. & Guo, X. Sodium-ion conduction in $\text{Na}_2\text{Zn}_2\text{TeO}_6$ solid electrolytes. *J. Power Sources* **402**, 513–518 (2018).
16. Sau, K. & Kumar, P. P. Role of Ion–Ion Correlations on Fast Ion Transport: Molecular Dynamics Simulation of $\text{Na}_2\text{Ni}_2\text{TeO}_6$. *J. Phys. Chem. C* **119**, 18030–18037 (2015).
17. Sau, K. Influence of ion–ion correlation on Na^+ transport in $\text{Na}_2\text{Ni}_2\text{TeO}_6$: molecular dynamics study. *Ionics (Kiel)*. **22**, 2379–2385 (2016).
18. Delmas, C., Fouassier, C., Réau, J.-M. & Hagenmuller, P. Sur de nouveaux conducteurs ioniques a structure lamellaire. *Mater. Res. Bull.* **11**, 1081–1086 (1976).
19. Balsys, R. J. & Lindsay Davis, R. The structure of $\text{Li}_{0.43}\text{Na}_{0.36}\text{CoO}_{1.96}$ using

- neutron powder diffraction. *Solid State Ionics* **69**, 69–74 (1994).
20. Berthelot, R., Pollet, M., Carlier, D. & Delmas, C. Reinvestigation of the OP4-(Li/Na)CoO₂-layered system and first evidence of the (Li/Na/Na)CoO₂ phase with OPP9 oxygen stacking. *Inorg. Chem.* **50**, 2420–2430 (2011).
 21. Ren, Z. *et al.* Enhanced thermopower in an intergrowth cobalt oxide Li_{0.48}Na_{0.35}CoO₂. *J. Phys. Condens. Matter* **18**, L379–L384 (2006).
 22. Yabuuchi, N. *et al.* A Comparative Study of LiCoO₂ Polymorphs: Structural and Electrochemical Characterization of O2-, O3-, and O4-type Phases. *Inorg. Chem.* **52**, 9131–9142 (2013).
 23. Komaba, S., Yabuuchi, N. & Kawamoto, Y. A New Polymorph of Layered LiCoO₂. *Chem. Lett.* **38**, 954–955 (2009).
 24. Vallée, C. *et al.* Alkali-Glass Behavior in Honeycomb-Type Layered Li_{3-x}Na_xNi₂SbO₆ Solid Solution. *Inorg. Chem.* **58**, 11546–11552 (2019).
 25. Shannon, R. D. Revised effective ionic radii and systematic studies of interatomic distances in halides and chalcogenides. *Acta Crystallogr. Sect. A* **32**, 751–767 (1976).
 26. Holzapfel, M. *et al.* Mixed layered oxide phases Na_xLi_{1-x}NiO₂: A detailed description of their preparation and structural and magnetic identification. *Solid State Sci.* **7**, 497–506 (2005).
 27. Pennycook, S. J. *et al.* Scanning Transmission Electron Microscopy for Nanostructure Characterization. in *Scanning Microscopy for Nanotechnology: Techniques and Applications* (eds. Zhou, W. & Wang, Z. L.) 152–191 (Springer, 2006).
 28. Pennycook, S. J. & Boatner, L. A. Chemically sensitive structure-imaging with a scanning transmission electron microscope. *Nature* **336**, 565–567 (1988).
 29. Pennycook, S. J., Varela, M., Hetherington, C. J. D. & Kirkland, A. I. Materials Advances through Aberration-Corrected Electron Microscopy. *MRS Bull.* **31**, 36–43 (2006).
 30. Kanyolo, G. M. & Masese, T. An Idealised Approach of Geometry and Topology to the Diffusion of Cations in Honeycomb Layered Oxide Frameworks. *Sci. Rep.* **10**, 13284 (2020).
 31. Li, Q. *et al.* K⁺-doped Li_{1.2}Mn_{0.54}Co_{0.13}Ni_{0.13}O₂: A novel cathode material with an enhanced cycling stability for lithium-ion batteries. *ACS Appl. Mater. Interfaces* **6**, 10330–10341 (2014).
 32. He, W. *et al.* Enhanced high-rate capability and cycling stability of Na-stabilized layered Li_{1.2}[Co_{0.13}Ni_{0.13}Mn_{0.54}]O₂ cathode material. *J. Mater. Chem. A* **1**, 11397–11403 (2013).

33. Li, N. *et al.* Incorporation of rubidium cations into $\text{Li}_{1.2}\text{Mn}_{0.54}\text{Co}_{0.13}\text{Ni}_{0.13}\text{O}_2$ layered oxide cathodes for improved cycling stability. *Electrochim. Acta* **231**, 363–370 (2017).
34. Zheng, J. *et al.* Li- and Mn-Rich Cathode Materials: Challenges to Commercialization. *Adv. Energy Mater.* **7**, (2017).
35. Dahiya, P. P., Ghanty, C., Sahoo, K., Basu, S. & Majumder, S. B. Effect of Potassium Doping on the Electrochemical Properties of $0.5\text{Li}_2\text{MnO}_3$ - $0.5\text{LiMn}_{0.375}\text{Ni}_{0.375}\text{Co}_{0.25}\text{O}_2$ Cathode. *J. Electrochem. Soc.* **165**, A2536–A2548 (2018).
36. Ding, X. *et al.* Cesium doping to improve the electrochemical performance of layered $\text{Li}_{1.2}\text{Ni}_{0.13}\text{Co}_{0.13}\text{Mn}_{0.54}\text{O}_2$ cathode material. *J. Alloys Compd.* **791**, 100–108 (2019).
37. Ates, M. N. *et al.* Mitigation of Layered to Spinel Conversion of a Li-Rich Layered Metal Oxide Cathode Material for Li-Ion Batteries. *J. Electrochem. Soc.* **161**, A290–A301 (2014).
38. Guan, L., Xiao, P., Lv, T., Zhang, D. & Chang, C. Improved Electrochemical Performance of $\text{Rb}_x\text{Li}_{1.27-x}\text{Cr}_{0.2}\text{Mn}_{0.53}\text{O}_2$ Cathode Materials via Incorporation of Rubidium Cations into the Original Li Sites. *J. Electrochem. Soc.* **164**, A3310–A3318 (2017).
39. Dong, J., Xiao, P., Zhang, D. & Chang, C. Enhanced rate performance and cycle stability of $\text{LiNi}_{0.8}\text{Co}_{0.15}\text{Al}_{0.05}\text{O}_2$ via Rb doping. *J. Mater. Sci. Mater. Electron.* **29**, 21119–21129 (2018).
40. Berthelot, R., Pollet, M., Doumerc, J. & Delmas, C. (Li/Ag) CoO_2 : A New Intergrowth Cobalt Oxide Composed of Rock Salt and Delafossite Layers. *Inorg. Chem.* **50**, 6649–6655 (2011).
41. Zhang, H., Arlego, M. & Lamas, C. A. Quantum phases in the frustrated Heisenberg model on the bilayer honeycomb lattice. *Phys. Rev. B* **89**, 024403 (2014).
42. Wang, M. & Tang, Y. B. A Review on the Features and Progress of Dual-Ion Batteries. *Adv. Mater.* **8**, 1703320 (2018).
43. Petříček, V., Dušek, M. & Palatinus, L. Crystallographic Computing System JANA2006: General features. *Z. Kristallogr. Cryst. Mater.* **229**, 345–352 (2014).
44. Matsubara, N. *et al.* Magnetism and Ion Diffusion in Honeycomb Layered Oxide $\text{K}_2\text{Ni}_2\text{TeO}_6$: First Time Study by Muon Spin Rotation & Neutron Scattering. arXiv. arXiv: 2003.05805 (2020).
45. Xue, L., Gao, H., Li, Y. & Goodenough, J. B. Cathode Dependence of Liquid-Alloy Na–K Anodes. *J. Am. Chem. Soc.* **140**, 3292–3298 (2018).
46. Guo, X., Zhang, L., Ding, Y., Goodenough, J. B. & Yu, G. Room-temperature liquid metal and alloy systems for energy storage applications. *Energy Environ. Sci. Soc.* **12**,

2605–2619 (2019).

47. Chen, C. –Y., Matsumoto, K., Kubota, K., Hagiwara, R. & Xu, Q. An Energy - Dense Solvent - Free Dual - Ion Battery. *Adv. Funct. Mater.*, <https://doi.org/10.1002/adfm.202003557> (2020).
48. Matsumoto, K., Okamoto, Y., Nohira, T. & Hagiwara, R. Thermal and Transport Properties of $\text{Na}[\text{N}(\text{SO}_2\text{F})_2]\text{--}[\text{N-Methyl-N-propylpyrrolidinium}][\text{N}(\text{SO}_2\text{F})_2]$ Ionic Liquids for Na Secondary Batteries. *J. Phys. Chem. C* **119**, 7648–7655 (2015).
49. Matsumoto, K., Hwang, J., Kaushik, S., Chen, C. –Y. & Hagiwara, R. Advances in sodium secondary batteries utilizing ionic liquid electrolytes. *Energy Environ. Sci.* **12**, 3247–3287 (2019).
50. Yamamoto, T., Matsumoto, K., Hagiwara, R. & Nohira, T. Physicochemical and Electrochemical Properties of $\text{K}[\text{N}(\text{SO}_2\text{F})_2]\text{--}[\text{N-Methyl-N-propylpyrrolidinium}][\text{N}(\text{SO}_2\text{F})_2]$ Ionic Liquids for Potassium-Ion Batteries. *J. Phys. Chem. C* **121**, 18450–18458 (2017).
51. Saito, M., Kimoto, K., Nagai, T., Fukushima, S., Akahoshi, D., Kuwahara, H., Matsui, Y., & Ishizuka, K. Local crystal structure analysis with 10-pm accuracy using scanning transmission electron microscopy. *J. Electron Microsc.* **53** 131–136 (2009).
52. Sau, K. & Kumar, P. P. Ion Transport in $\text{Na}_2\text{M}_2\text{TeO}_6$: Insights from Molecular Dynamics Simulation. *J. Phys. Chem. C* **119** 1651–1658 (2015).
53. Plimpton, S. Fast parallel algorithms for short-range molecular dynamics. *J. Comp. Phys.* **117** 1–19 (1995).

Acknowledgements

We thank Ms. Shinobu Wada and Mr. Hiroshi Kimura for the unrelenting support in undertaking this study. We gratefully acknowledge Ms. Kumi Shiokawa, Mr. Masahiro Hirata and Ms. Machiko Kakiuchi for their advice and technical help as we conducted the syntheses, electrochemical and XRD measurements. This work was conducted in part under the auspices of the Japan Society for the Promotion of Science (JSPS KAKENHI Grant Number 19K15685), Sumika Chemical Analyses Services (SCAS) Co. Ltd., National Institute of Advanced Industrial Science and Technology (AIST) and Japan Prize Foundation.

Data availability

The data that support the findings of this study (Supplementary materials including experimental (methods) details) will be availed during the production stage.

Competing interests

The authors declare no competing interests.